Role of the Conserved Arginine Pair in Proton and Electron Transfer in Cytochrome *c* Oxidase†

Jie Qian,‡,§ Denise A. Mills,‡ Lois Geren,|| Keifei Wang,|| Curt W. Hoganson,|| Bryan Schmidt,‡ Carrie Hiser,‡ Gerald T. Babcock,# Bill Durham,|| Francis Millett,*,|| and Shelagh Ferguson-Miller*,‡

Departments of Biochemistry and Chemistry, Michigan State University, East Lansing, Michigan 48824-1319, and Department of Chemistry, University of Arkansas, Fayetteville, Arkansas 72701

Received December 18, 2003; Revised Manuscript Received February 24, 2004

ABSTRACT: A hydrogen-bonded network is observed above the hemes in all of the high-resolution crystal structures of cytochrome oxidases. It includes water and a pair of arginines, R481 and R482 (*Rhodobacter sphaeroides* numbering), that interact directly with heme *a* and the heme a_3 propionates. The hydrogen-bonded network provides potential pathways for proton release. The arginines, and the backbone peptide bond between them, have also been proposed to form part of a facilitated electron transfer route between Cu_A and heme *a*. Our studies show that mutations of R482 (K, Q, and A) and R481 (K) retain substantial activity and are able to pump protons, but at somewhat reduced rates and stoichiometries. A slowed rate of electron transfer from cytochrome *c* to Cu_A suggests a change in the orientation of cytochrome *c* binding in all but the R to K mutants. The mutant R482P is more perturbed in its structure and is altered in the redox potential difference between heme *a* and Cu_A: +18 mV for R482P and +46 mV for the wild type (heme *a* − Cu_A). The electron transfer rate between Cu_A and heme *a* is also altered from 93000 s^{-1} in the wild type to 50 s^{-1} in the oxidized R482P mutant, reminiscent of changes observed in a Cu_A-ligand mutant, H260N. In neither case is the ∼2000-fold change in the rate accounted for by the altered redox potentials, suggesting that both cause a major modification in the path or reorganization energy of electron transfer.

Respiration involves the transfer of electrons through a series of membrane protein complexes resulting in the production of an electrochemical gradient across a membrane, which is used to drive the synthesis of ATP as an energy source for the cell. Cytochrome *c* oxidase (C*c*O)[1] is the terminal electron transfer protein in most aerobic organisms; using oxygen as the final electron acceptor, C*c*O generates a proton gradient by consuming protons from the interior to make water and translocating one proton per electron across the membrane.

Pathways for the uptake of protons from the interior side of the membrane to the level of the active site (heme a_3/Cu_B) have been established. However, the route by which the protons are released to the exterior side is not well-defined. An essential glutamate (E286) in the vicinity of the hemes may undergo a conformational change during the catalytic cycle and facilitate proton movement to the region above the hemes (*1*−*5*). This region, including the heme propionates, is proposed to provide a site, or sites, for proton binding to facilitate electron transfer-coupled proton movement (*1*, *6*). Changes in conserved amino acids in this region might be expected to perturb proton pumping and/or alter the redox behavior of the hemes (*7*).

The heme propionates participate in a hydrogen-bonded network involving a number of water molecules at the interface of subunit I and subunit II, based on the three-dimensional structure of beef heart (bov) *Paraccocus denitrificans* (*Pd*) and *Rhodobacter sphaeroides* (*Rs*) C*c*O (*8*−*10*) (Figure 1). A pair of highly conserved arginines, R481 and R482 (*Rs* C*c*O numbering), are involved in this network and are directly hydrogen-bonded to the heme propionates and to the ligands of a non-redox-active Mg site. The peptide backbone between them is hydrogen-bonded to the dinuclear Cu_A site. The nitrogen atoms of R482 are hydrogen-bonded to the A- and D-propionate groups of heme *a*, while the two terminal nitrogens of R481 are hydrogen-bonded to the D-propionate of heme a_3 as well as the D-propionate of heme *a* (Figure 1). At least one water connects R481 to the Mg ligand, D412, and another water connects the side chain of R482 to $E254^{II}$ (*9*), a bridging ligand between the Cu_A and Mg sites. Mg has been proposed to play a role in the water exit channel in C*c*O (*11*) and possibly in a proton exit route (*12*). However, when the Mg ligands are mutated and the Mg is perturbed or lost, the oxidase is still capable of proton

† Supported by National Institutes of Health Grants GM 26916 (to S.F.-M.), GM 20488 (to F.M., L.G., and B.D.), and NCRR COBRE 1 P20 RR15569 (F.M. and B.D.).

* To whom correspondence should be addressed. S.F.-M.: telephone, 517-353-0199; fax, 517-353-9334; e-mail, fergus20@pilot.msu.edu. F.M.: telephone, 479-575-4999; fax, 479-575-4049; e-mail, millett@uark.edu.

‡ Department of Biochemistry, Michigan State University.

§ Current address: Abbott Laboratories, 200 Abbott Park Road, Abbott Park, IL 60064.

|| Department of Chemistry, University of Arkansas.

Department of Chemistry, Michigan State University (deceased).

[1] Abbreviations: C*c*O, cytochrome *c* oxidase; EPR, electron paramagnetic resonance; PCR, polymerase chain reaction; *Pd*, *Paracoccus denitrificans*; *Rs*, *Rhodobacter sphaeroides*; RCR, respiratory control ratio; RuC*c*, ruthenium complex labeled cytochrome *c*.

10.1021/bi036279o CCC: $27.50
Published on Web 04/22/2004

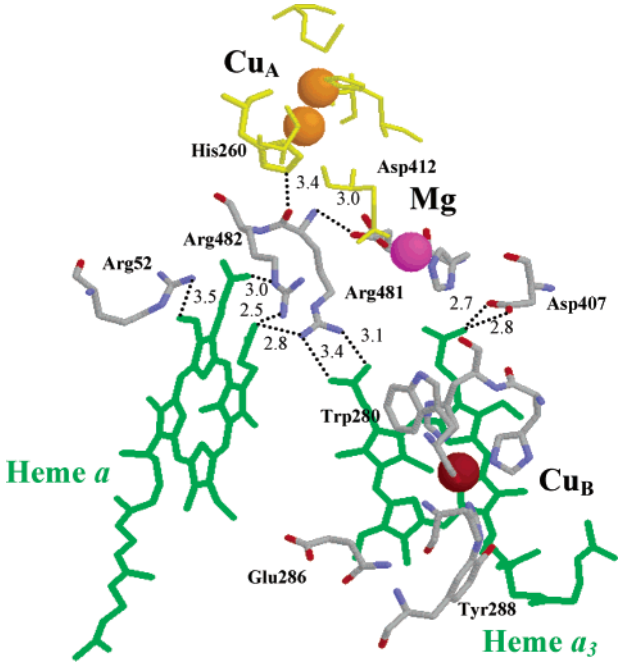

FIGURE 1: Structure of *R. sphaeroides* C*c*O above the hemes showing the position of the pair of arginines and their interaction with the heme propionates and the connection to subunit II amino acids (yellow) and the dinuclear Cu_A and redox-inactive Mg. This figure was produced using Rasmol from the crystal structure 1M56 (*10*).

pumping (*12*, *13*). Studies of site-directed mutants of the arginine pair in the *bo*$_3$ quinol oxidase in *Escherichia coli* membranes suggest that mutations of R482 do not destroy proton pumping but that the R481 mutants are more disruptive both structurally and functionally (*14*). The question remains whether R482 and R481 have only a structural role in stabilizing the hemes and the subunit I/II interface or whether they are crucial for rapid proton transfer or in maintaining the redox potentials of the hemes.

The question has also been raised as to whether the arginine pair and their connecting peptide backbone play a role in electron transfer. Cytochrome *c* is the initial electron donor for C*c*O and delivers its electron to the dinuclear Cu_A site. From there the electron is rapidly transferred [9×10^4 s^{-1} (*15*−*17*)] to heme *a*, facilitated in part by a low reorganization energy due to the polar environment of heme *a* (*18*). The route of electron transfer from Cu_A to heme *a* appears to be strongly preferred over the route to the almost equidistant heme *a*$_3$ (*19*). This raises the issue of whether there is any role of the protein in directing or facilitating the electron transfer process (*20*, *21*). The peptide backbone of the arginine pair is within hydrogen-bonding distance of His260, a ligand of one of the coppers at the Cu_A site, and the long arginine side chains reach down to the hemes as if forming an electron wire (*20*). However, the R481 appears to interact with the propionate groups of both heme *a* and heme *a*$_3$. The present study addresses these questions regarding the structural and functional role of the arginine pair by analysis of the spectral, catalytic, and proton pumping properties of mutant forms of *R. sphaeroides* C*c*O including R481K and R482K, R482Q, R482A, and R482P. The results indicate an important structural role and potential involvement in proton and electron transfer.

Chart 1

	P	R	R	Y	I	D
WT	5'-CCG	CGG	CGC	TAC	ATC	GAC-3'
R482K	5'-CCG	CGG	AAA	TAC	ATC	GAC-3'
R482A	5'-CCG	CGG	GCC	TAC	ATC	GAC-3'
R482Q	5'-CCG	CGG	CAA	TAC	ATC	GAC-3'
R482P	5'-CCG	CGG	CCC	TAC	ATC	GAC-3'
R481K	5'-CCG	AAG	CGC	TAC	ATC	GAC-3'

MATERIALS AND METHODS

Site-Directed Mutagenesis. Site-directed mutants were constructed using PCR overlapping extension methods (*22*). All of the oligonucleotide primers were synthesized by the Michigan State University Macromolecular Structural Facility, East Lansing, MI. The primers used to create the mutants are shown in Chart 1.

The 692 bp final PCR product was digested with *Sal*I/*Hin*dIII, and then the 519 bp fragment was subcloned into pND38, a plasmid that contains part of the subunit I gene of cytochrome *c* oxidase. The pND38 plasmid with the mutation was digested with *Bgl*II/*Hin*dIII, and the 652 bp fragment was subcloned to pJS3-X6H$_2$, a plasmid containing the entire subunit I gene with a 6-histidine tag at the C-terminus of the COXI gene (*23*). The subsequent subcloning and conjugation were conducted as previously described (*24*). All of the mutants were subjected to DNA sequencing by the Michigan State University Sequencing Facility, East Lansing, MI, and no secondary mutations were found. Amino acid numbering is for *Rs* C*c*O subunit I unless there is a superscript (e.g., for a subunit II residue, E254^{II}).

Enzyme Purification. R. sphaeroides cells, overexpressing cytochrome *c* oxidase, were grown in Sistrom's media as described (*25*, *26*), and the C*c*O was purified by Ni-NTA affinity column chromatography (*24*, *27*) with some modifications. The protein, after Ni-NTA affinity column chromatography (*28*), was further washed with 0.1% lauryl maltoside, 10 mM Tris-HCl, and 40 mM KCl, pH 8.0, three times by a Centricon-50 concentrator (Amicon) to remove Ni−histidine. Prior to reconstitution into vesicles, an ion-exchange chromatography purification step was carried out using two DEAE columns (Tosohaas DEAE-5PW 10 μm particle size, 8 mm $\times$ 7.5 cm) in tandem using an FPLC as before (*25*, *27*, *28*).

Reconstitution of Cytochrome c Oxidase. Cytochrome *c* oxidase vesicles (COVs) were prepared as described (*25*, *26*) with 20 mg/mL asolectin and 2 μM oxidase with 3% sodium cholate. The vesicles were dialyzed against 100 volumes of 75 mM HEPES−KOH, pH 7.4, 14 mM KCl, and 0.1% cholate for 5−6 h, 100 volumes of 75 mM HEPES−KOH, pH 7.4, and 14 mM KCl for 12 h, 100 volumes of 50 mM HEPES−KOH, pH 7.4, 25 mM KCl, and 15 mM sucrose for 5−6 h, and 500 volumes of 50 μM HEPES−KOH, pH 7.4, 45 mM KCl, and 44 mM sucrose for 5 h, with repetition of the last dialysis step. Oxygen consumption assays were performed in 10 mM HEPES−KOH, pH 7.4, 41 mM KCl, and 38 mM sucrose for the reconstituted enzymes in order to determine the respiratory control ratio (RCR), which is a test of whether the COVs are able to produce and maintain a membrane potential and pH gradient and whether the

Scheme 1

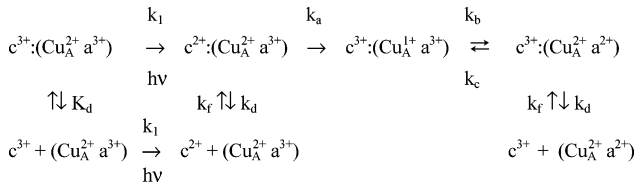

enzymes are inserted correctly (*24*, *26*). The RCR is the ratio of the uncontrolled rate (in the presence of uncoupler) over the controlled rate (in the absence of any ionophores), which is expected to be 1 for the free enzyme.

Stopped-Flow Proton Pumping Assay. Measurements of cytochrome *c* oxidation were made in an Olis rapid-scanning stopped-flow spectrophotometer in the absence of phenol red with reduced cytochrome c^{2+}. Turnover rates were calculated from exponential fitting of the decrease in absorbance at 550 nm and then multiplying this k_{obs} (s^{-1}) by the concentration of cytochrome c^{2+} [from $\epsilon_{550} = 17000\ M^{-1}\ cm^{-1}$ from the difference spectra (*29*) and cell path length of 0.4 cm] divided by the [aa_3]. Proton pumping assays were conducted on the Olis-rsm spectrophotometer as described previously (*28*). The buffer was 50 μM HEPES−KOH, pH 7.4, 45 mM KCl, and 44 mM sucrose with phenol red as the pH-sensitive dye at 100 μM final concentration. There is a 1:1 stoichiometry of substrate protons to electrons, and therefore the increase in absorbance (alkalinization on the outside) in the presence of uncoupler (CCCP) is representative of the electrons consumed. Therefore, the H^+/e^- ratio is derived by comparing the amplitude of the absorbance changes with valinomycin (H^+: acidification) with that of uncoupler (e^-: alkalinization). The traces for phenol red absorbance are corrected for the mixing artifact observed in the controlled state with no ionophores, which is shown as uncorrected data.

Flash-Activated Ruthenium Cytochrome c Kinetics Assay. Ruthenium fast kinetic measurements were carried out as described in Geren et al. (*16*) and Wang et al. (*30*) using the Ru-55-C*c* derivative of horse heart cytochrome *c*. The reaction of cytochrome *c* was monitored at 550 nm using an extinction coefficient of $\Delta\epsilon_{550} = 18.5\ mM^{-1}\ cm^{-1}$ (*31*). The reaction of Cu_A was monitored at 850 nm using $\Delta\epsilon_{850} = 2.0\ mM^{-1}\ cm^{-1}$ (*32*), and the reduction of heme *a* was measured at 605 nm using $\Delta\epsilon_{605} = 16\ mM^{-1}\ cm^{-1}$ (*33*). Reaction solutions typically contained 3−10 μM Ru-C*c*, 5−20 μM C*c*O, 10 mM aniline, and 1 mM 3CP in 5 mM Tris-HCl, pH 8.0, at 22 °C. The aniline and 3CP functioned as sacrificial electron donors to reduce Ru(III) and prevent the back-reaction with heme Fe(II). The ionic strength was adjusted by adding sodium chloride. The transients were fitted to appropriate theoretical equations for Scheme 1 as described by Geren et al. (*16*), and the reported errors are the estimated standard deviations.

Optical Spectroscopy. The dithionite-reduced minus ferricyanide-oxidized C*c*O spectra of the purified enzyme were recorded with a Perkin-Elmer Lambda 40P UV/visible spectrometer at 25 °C. For measuring the 850 nm band, at least 30 μM oxidized C*c*O was used with the background reduced spectra subtracted.

Other Assays. Determination of catalytic activity was measured as described (*24*). Continuous X-band EPR spectra were measured using a Bruker ESP-300E equipped with a TE102 cavity resonator. The temperature was maintained at 10 K using an Oxford ESR900 helium cryostat. Spectra were measured at either 2 or 20 mW of microwave power and a modulation amplitude of 12.7 G.

Table 1: Activity and Spectral Characteristics of the C*c*O Arginine Mutants Compared to Wild Type[a]

C*c*O	activity of enzyme, $e^-\ s^{-1}\ aa_3^{-1}$ (% WT)	ϵ_{850nm}, $mM^{-1}\ cm^{-1}$
WT	1500 (100)	2.0
R482K	1400 (93)	2.0
R482Q	600 (40)	1.5
R482A	480 (32)	2.0
R482P	60 (4)	1.0
R481K	1500 (100)	2.0

[a] Steady-state activity measurements were made in a Gilson oxygraph with 30 μM horse heart cytochrome *c*, 3 mM ascorbate, 1 mM TMPD, 2 mg of asolectin lipids, and 0.05% lauryl maltoside. The extinction coefficient of Cu_A at 850 nm was calculated from fully oxidized C*c*O minus fully reduced C*c*O (see Figure 2B) (*43*).

RESULTS

Overall Steady-State Activity. The isolated mutants all have a lower steady-state activity compared to wild type with the exception of R481K and R482K (Table 1). The mutation of R482 to a small hydrophobic alanine causes considerable loss of steady-state activity but without affecting Cu_A binding. The R482P mutant has the lowest activity, showing only 4% of wild-type steady-state oxygen consumption activity. Part of this loss is due to the presence of dissociated forms, but a reasonable fraction (∼50%, Table 1) appears to have native Cu_A and heme *a* content (Figure 2). Therefore, the considerable loss of activity in the R482P mutant is not just an effect of disassembled protein.

Optical Spectra. Some loss of heme was noticed in all but the conservative mutations of R481K and R482K, after initial purification by metal affinity chromatography. However, after FPLC purification the resulting enzyme, from each of the mutants, has a spectrum similar to that of the wild type with a Soret peak of reduced C*c*O at 445 nm and an α peak at 606 nm, which is distinctive for reduced heme *a* (Figure 2A). However, for R482P, the spectrum is considerably more disrupted with a blue-shifted Soret and α peak, suggesting some perturbation of both hemes due to structural disturbance.

Measurement of the absorbance in the near-IR range of the ferricyanide-oxidized C*c*O, with subtraction of the dithionite-reduced C*c*O background, gives a broad peak centered at 850 nm for wild-type C*c*O that has been assigned to Cu_A (*34*). Using the absorbance of fully reduced C*c*O at 605 nm with a known extinction coefficient ($38\ mM^{-1}\ cm^{-1}$) the concentration of the protein can be calculated. This is then used to calculate an apparent extinction coefficient for Cu_A. A ϵ_{850} of $2\ mM^{-1}\ cm^{-1}$ was obtained for the wild type (Table 1). All mutants show similar visible spectra of Cu_A to that of the wild type and the C*c*O mutant R481K, with the broad peak being centered at 850 nm (Figure 2B). R482K, R481K, and R482A have an apparent ϵ_{850} of 2.0 $mM^{-1}\ cm^{-1}$, the same as that of the wild type, while R482Q and R482P have an apparent ϵ_{850} of 1.5 and 1.0 (Table 1), respectively, implying that there is loss of Cu_A in R482Q (25%) and R482P (∼50%), probably due to some loss of subunit II.

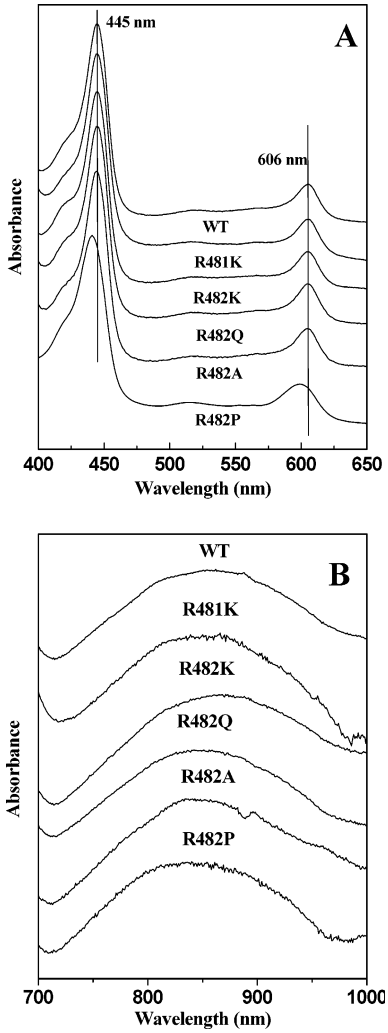

FIGURE 2: Visible spectra of reduced wild type and R481/2 C*c*O mutants showing (A) normal Soret (445 nm) and α (606 nm) bands in all but R482P. C*c*O (~2 μM) was reduced with sodium dithionite. (B) Broad Cu_A spectra in the 700−1000 nm near-IR region of oxidized C*c*O (with ferricyanide) minus reduced C*c*O (with sodium dithionite).

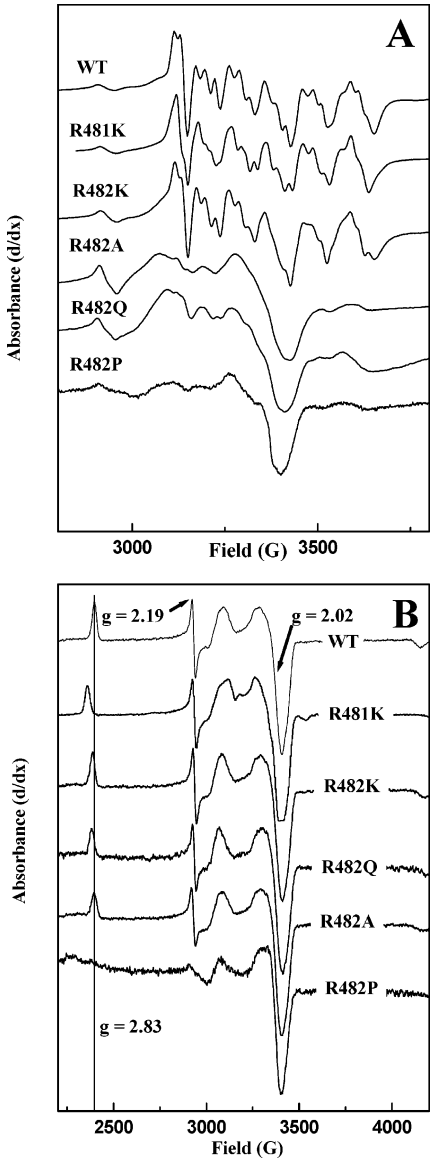

FIGURE 3: Structural analysis of the arginine mutants by examination of the Cu_A and Mg metal sites. Electron paramagnetic resonance (EPR) spectra of C*c*O with (A) enrichment with Mn shows six-line hyperfine Mn signals at $g = 2.0$. (B) Enrichment in Mg reveals the Cu_A EPR spectra. Additionally, oxidized heme *a* is observed at, or close to, the vertical line depicting the $g = 2.83$ signal.

Mg Site and Cu_A and Heme a Environments: EPR Spectra. The Mg site and Cu_A and heme *a* environments can be monitored by EPR (electron paramagnetic resonance) spectroscopy. The oxidized forms of Cu_A and heme *a* are paramagnetic (have an unpaired electron), and the Mg site can be substituted with paramagnetic Mn when *R. sphaeroides* is grown under high [Mn]/low [Mg] conditions (*24*, *25*). Compared to the distinctive six-line hyperfine Mn signals at the $g = 2.0$ region for the wild type (Figure 3A), the R482K spectrum shows a slight alteration in the Mn signal. Further comparison by integration of the first peak of the wild type and R482K spectra indicates that 65% of the Mn is present in the Mg site in the R482K mutant. The C*c*O mutants R482A, R482Q, and R482P failed to bind Mn, resulting in the appearance of the Cu_A signals which are normally masked. These results suggest that the nonconservative mutants lose substantial Mn/Mg binding ability. The conservative mutants, R482K and R481K, undergo a minor structural change at the Mg site as seen in subtle changes of the EPR hyperfine splitting, suggesting that these have slight alterations in the interactions of ligands with the metal. In R481K the changes are more marked and show some similarity to the Mn spectrum in the reduced enzyme (*35*).

Growth of *R. sphaeroides* in high [Mg]/low [Mn] media removes the Mn signal and allows that of Cu_A and heme *a* to be observed. Characteristic Cu_A signals at $g = 2.19$ and $g = 2.02$ are seen for the wild-type C*c*O and all of the mutants. These signals are weaker for the R482P C*c*O mutant, probably because of a decreased amount of Cu_A (Table 1), and somewhat altered showing some disturbance of the dinuclear Cu_A site (Figure 3B). Oxidized heme *a* in the wild-type *Rs* C*c*O shows a characteristic EPR signal at $g = 2.83$ (Figure 3B) distinct from the bovine C*c*O at $g = 3.03$ (*25*). Interestingly, several of the R482 mutants, most notably R482K and R482Q as well as R481K, have a spectral shift of heme *a* to $g = 2.85$, toward the bovine value, and similar to that of the mutant H260N (*36*) C*c*O, which is a ligand of Cu_A (Figure 1). R482P does not show a peak in this region.

Table 2: Activity of R482 Mutants Reconstituted into Vesicles and Proton Pumping Stoichiometry from Stopped-Flow Measurements[a]

	activity, $e^- s^{-1} aa_3^{-1}$			
COVs	controlled	uncontrolled	RCR[b]	H^+/e^- [c]
WT	80	670	8.4	0.9
R482K	82	840	10.2	0.8
R482Q	61	460	7.5	0.8
R482A	58	390	6.8	0.6
R482P	5	15	3.0	0.0

[a] See Figure 4. [b] RCR = respiratory control ratio = uncontrolled rate/controlled rate. [c] H^+/e^- represents the efficiency of proton pumping (1.0 is the expected efficiency). Errors in these measurements are expected to be at least ±0.2.

Respiratory Control and Proton Pumping Activity. Reconstitution of the arginine mutants, purified by an additional FPLC chromatography step, gave normal respiratory control ratios (RCR > 1) as measured under steady-state conditions for oxygen consumption (Table 2), suggesting that these mutants have incorporated into the asolectin lipid vesicles properly. The RCR for R482P is low due to the low activity of this mutant so that even the uncontrolled rate, in the absence of a membrane potential or pH gradient, is only capable of attaining 2% of the wild-type activity. Proton pumping is observed as a decrease in absorbance in the presence of the ionophore valinomycin, which relieves the membrane potential ($\Delta\Psi$). When uncoupler (CCCP) is added, only an increase in absorbance is observed, which represents alkalinization due to the protons consumed on the inside for the reduction of O_2 to H_2O. The results show that all of the mutants, with the exception of R482P, have good efficiency of proton pumping, evidenced by the H^+/e^- approaching 1 (0.8−0.6) (Figure 4, Table 2). However, it is possible that the observed lower rates of pumping (and lower catalytic turnover) are due to rate limitation by an altered proton exit path. The R482P mutant may have a considerably disturbed structure such that it is unable to efficiently pump protons against a pH gradient.

Photoinduced Electron Transfer Measurements. Rapid electron transfer between C*c* and the R482 C*c*O mutants was studied using Ru-55-C*c*, which contains a ruthenium trisbipyridine complex covalently attached to lysine 55 on the bottom surface of C*c* away from the binding domain. The ruthenium complex on Ru-55-C*c* does not affect the interaction with C*c*O (*37*). The Ru(II) group is photoexcited to a metal-to-ligand charge transfer state, Ru(II*), which rapidly transfers an electron to heme *c* (*38*). Ru-55-C*c* forms a 1:1 complex with *R. sphaeroides* C*c*O at low ionic strength, allowing measurement of electron transfer from photoreduced heme *c* to Cu_A with a rate constant k_a of 40000 s^{-1}, followed by electron transfer from Cu_A to heme *a* with rate constant k_b (Scheme 1) (*37*). The value of k_b is larger than that of k_a and thus could not be measured using Ru-55-C*c*. However, k_b was measured to be 90000 s^{-1} using a ruthenium dimer which reduces Cu_A directly within 1 μs (*39*). The ratio of reduced heme *a* to Cu_A, after equilibrium is reached in about 1 ms, is 6.1, indicating that the equilibrium constant for electron transfer between Cu_A and heme *a* is $K = k_b/k_c = 6.1$ (Table 3) (*37*). This indicates that the difference in heme *a* and Cu_A redox potentials, ΔE (heme *a* − Cu_A), is +46 mV in the state where heme a_3 and Cu_B both remain oxidized. The rate constant k_a of electron transfer from cytochrome *c* to Cu_A within the C*c*/C*c*O complex is not altered by increasing ionic strength (Figure 5A), but as the ionic strength is raised, the amplitude of the fast phase decreases, indicating complex dissociation. Above 50 mM ionic strength a new slow phase appears due to the bimolecular reaction of uncomplexed Ru-55-C*c* with C*c*O (Scheme 1). The pseudo-first-order rate constant k_{obs} of the slow phase

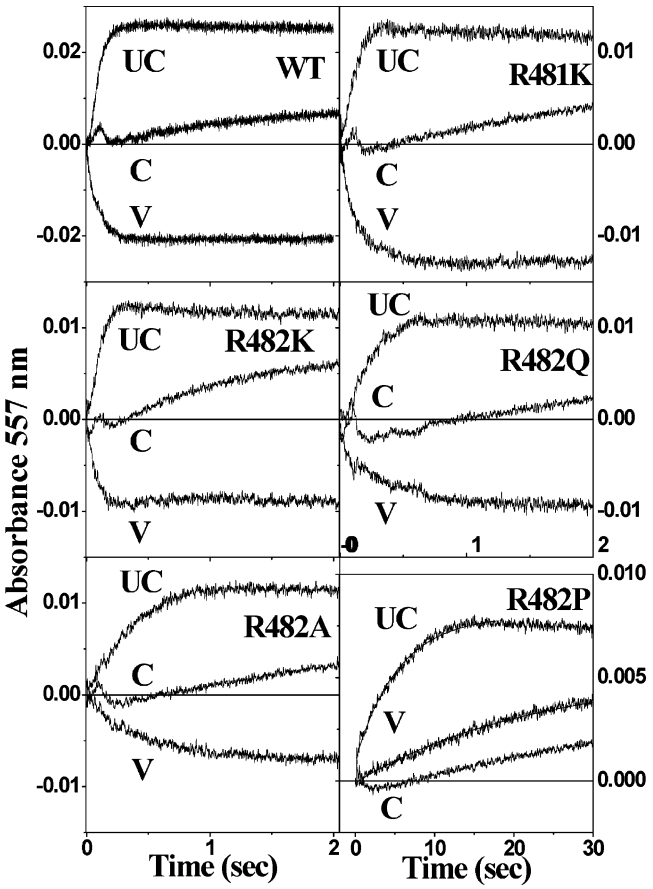

FIGURE 4: Normal proton pumping is observed for all of the mutants with the exception of R482P. Proton pumping is detected in a stopped-flow spectrophotometer using a phenol red dye on the outside of the vesicles to monitor proton changes using the absorbance change at 557 nm, which is close to the maximal absorbance of the dye and is an isosbestic point for cytochrome *c*. Phenol red (100 μM) changes on the outside of COVs (0.15 μM C*c*O) are shown: C = controlled (with no ionophores), V = with 2 μM valinomycin (acidification of the outside gives a decrease in dye absorbance), UC = uncontrolled with 2 μM valinomycin + 5 μM CCCP (alkalinization gives an increase in dye absorbance).

Table 3: Rapid Kinetics Reaction of Ru-55-C*c* with C*c*O Arginine Mutants[a]

C*c*O	k_a (s^{-1}) C*c* → Cu_A	k_b (s^{-1}) Cu_A → *a*	k_2 ($\mu M^{-1} s^{-1}$)	*K*	ΔE (mV) (*a* − Cu_A)
WT	40000	93000	310	6.1 ± 1.0	46 ± 4
R482K	50000	>60000	170	3.0 ± 1.0	28 ± 8
R482Q	8800	3400	81	5.0 ± 1.0	41 ± 5
R482A	7600	>4500	27	5.4 ± 1.0	43 ± 5
R482P		50	64	2.0 ± 1.0	18 ± 10

[a] The rate constants k_a for electron transfer from heme *c* to $Cu_A$and k_b for electron transfer from Cu_A to heme *a* were measured for 1:1 complexes between Ru-55-C*c* and C*c*O mutants in 5 mM Tris-HCl, pH 8.0 at 23 °C. The second-order rate constant k_2 was measured in 5 mM Tris-HCl, pH 8.0, and 90 mM NaCl. The equilibrium constant for electron transfer between Cu_A and heme *a*, $K = k_b/k_c$, and the difference in redox potentials, ΔE, were independent of ionic strength. The error limits in k_a, k_b, and k_2 are ±20%.

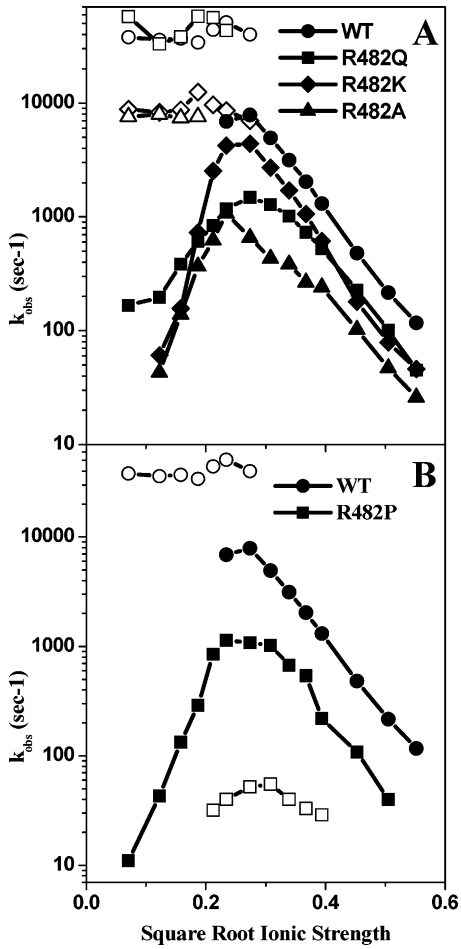

FIGURE 5: Ionic strength dependence of the reactions between Ru-55-C*c* and C*c*O mutants. The solutions contained 10 μM Ru-55-C*c*, 16 μM C*c*O in 5 mM Tris-HCl, pH 8.0, 0−300 mM NaCl, 10 mM aniline, and 1 mM 3CP. (A) The observed first-order rate constants k_{obs} for the fast phase (open symbols) and the slow biomolecular phase (solid symbols) are plotted as a function of ionic strength for the indicated derivatives. (B) For the R482P mutant, the observed rate constant k_{obs} for electron transfer from heme *c* to Cu_A and the rate constant k_b for electron transfer from Cu_A to heme *a* are both plotted.

reaches a maximum at 75 mM ionic strength and then decreases with further increases in ionic strength (Figure 5B). At ionic strengths above 90 mM, k_{obs} increases linearly with C*c*O concentration, allowing measurement of a second-order rate constant k_2 (Table 3) (*37*).

The conservative mutation R482K does not significantly affect the rate constant k_a for electron transfer from photoreduced heme *c* to Cu_A at low ionic strength and decreases the second-order rate constant k_2 at 90 mM ionic strength by only a factor of 1.8 (Figure 5, Table 3). The transition between intracomplex and bimolecular kinetics occurs at nearly the same ionic strength as wild-type C*c*O, indicating that there is little effect of the R482K mutant on the dissociation constant K_d of the complex (Figure 5). However, the equilibrium constant *K* for electron transfer between Cu_A and heme *a* is decreased to 3.0, indicating that the difference in redox potentials, ΔE, is 28 mV (Table 3).

The R482A mutation decreases the value of k_a by about 5-fold compared to wild-type C*c*O and also decreases the second-order rate constant k_2 by 11-fold at 90 mM ionic strength. The transition between intracomplex and biomolecular kinetics occurs at a lower ionic strength than for wild-type C*c*O, indicating a larger dissociation constant for the complex (Figure 5). As with the wild-type C*c*O, the observed rate constant, k_{obs}, for reduction of heme *a* for R482K and R482A was the same as that for oxidation of heme *c* at low ionic strength, and it was only possible to determine a lower limit for k_b (Table 3). However, for the R482Q mutant at low ionic strength, the rate constant for heme *a* reduction measured at 605 nm is smaller than that for oxidation of heme *c*, 3400 s^{-1} vs 8800 s^{-1}, respectively (Table 3). This result indicates that the rate constant k_a for electron transfer from heme *c* to Cu_A is 8800 s^{-1} and the rate constant k_b for electron transfer from Cu_A to heme *a* is 3400 s^{-1}.

The kinetics of the R482P mutant were significantly different from that of wild-type C*c*O and the other R482 mutants. The observed rate constant k_{obs} for electron transfer from heme *c* to Cu_A was very small at low ionic strength, 10 s^{-1}, increased to a maximum of 1140 s^{-1} at 55 mM ionic strength, and then decreased with further increases in ionic strength (Figure 5B). This result suggests that the complex between Ru-55-C*c* and R482P C*c*O is very poorly oriented for electron transfer at low ionic strength but can achieve a more favorable orientation at higher ionic strength. Over the entire ionic strength range the rate constant for reduction of Cu_A, measured at 830 nm, was the same as that for oxidation of heme *c* measured at 550 nm. An example is shown in Figure 6A, where the rate constant for electron transfer from heme *c* to Cu_A is 1100 s^{-1} at 75 mM ionic strength. The true intracomplex rate constant, k_a, is larger than the pseudo-first-order rate constant k_{obs} at this ionic strength. The reduction of Cu_A is followed by a much slower reoxidation, which is paralleled by the reduction of heme *a* measured at 605 nm (Figure 6B). This slow phase is therefore due to electron transfer from Cu_A to heme *a* with rate constant k_b. The value of k_b is 50 s^{-1} at 75 mM ionic strength and is nearly independent of ionic strength (Figure 5B, Table 3). After equilibrium is reached in 100 ms, Cu_A is 67% oxidized (Figure 6B), from which it can be estimated that the equilibrium constant *K* for electron transfer from Cu_A to heme *a* is 2.0 and the ΔE value (heme *a* − Cu_A) is +18 mV. This estimate does not depend on the extinction coefficient of Cu_A or the possibility that some of the Cu_A is lost. Any enzyme missing Cu_A would not react with Ru-55-C*c* and would not contribute to the absorbance transient signals.

DISCUSSION

It is perhaps surprising that such highly conserved residues as R481 and R482 should, upon mutagenesis, retain substantial activity and integrity. Even with loss of Mg in the R482Q and R482A mutants, reasonable steady-state activity is retained. This is consistent with studies on mutants of the Mg ligands, such as D412A, which also have significant activity despite loss of the Mg (*12*, *13*). However, in the intrinsic rate measurements, changes of 6-fold (*c* to Cu_A) and as much as 30-fold (Cu_A to heme *a*) are observed for the mutants (R482Q/A) where the charge is altered. Proline at that position appears to cause a large local conformational change particularly affecting the heme *a* site and the subunit I/II interface.

General Effects from Mutation of the Arginines. When R482 is mutated to a lysine, the enzyme is essentially wild

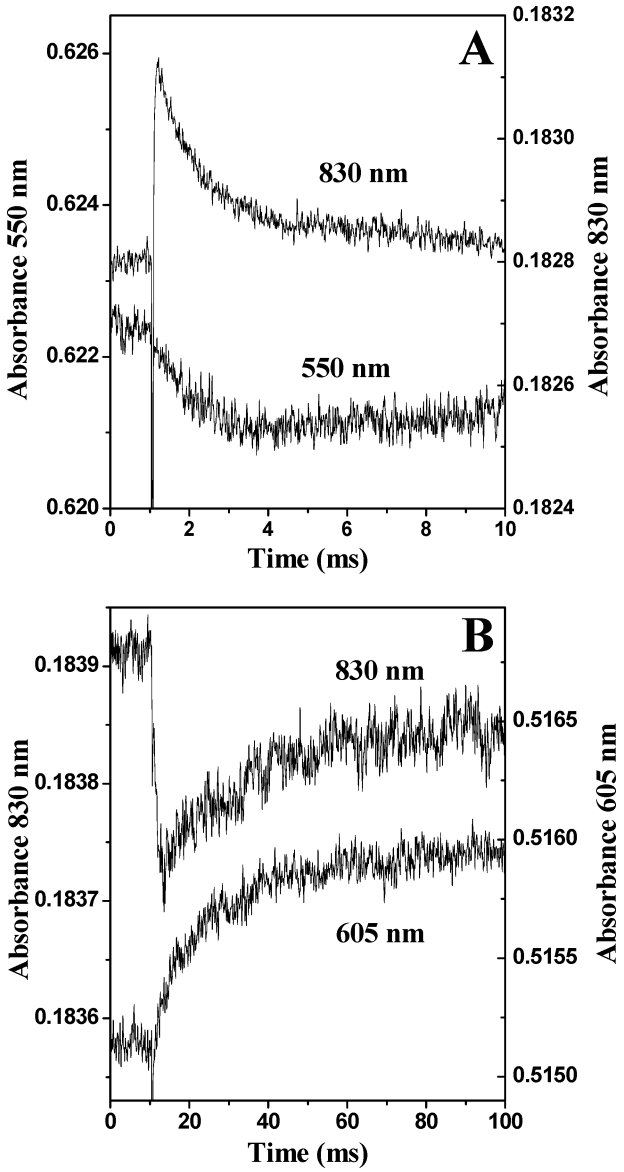

FIGURE 6: Photoinduced electron transfer from Ru-55-C*c* to R482P C*c*O. The solution contained 10 μM Ru-55-C*c*, 16 μM C*c*O in 5 mM Tris-HCl, pH 8.0, 10 mM aniline, 1 mM 3CP, and 70 mM NaCl. (A) 550 nm (C*c*) and 830 nm (Cu_A) transients at 10 ms time scale. (B) 830 and 605 nm (heme *a*) transients at 100 ms time scale. The k_{obs} rate constant for electron transfer from C*c* to Cu_A is 1100 s^{-1}, while the rate constant k_b for electron transfer from Cu_A to heme *a* is 50 s^{-1}.

type in many respects, presumably because this is a conservative replacement retaining the positive charge and the hydrogen bonding. However, the amino acid side chain length is different, as is the electrostatic charge distribution. The purified R482Q mutant of *Rs* C*c*O has somewhat lower activity, ~40% of the wild type, than observed in studies of the *E. coli* bo_3 oxidase in the membranes (*14*). Both results suggest that there is not a strict requirement for a protonatable side chain at this position or a positive charge. However, the arginine replacement with N or Q still allows hydrogen bonding, and this may be a more important property, as the hydrophobic mutants, R482A and R482P, have much lower activities [although the R482L mutant of the bo_3 oxidase in *E. coli* membranes was reported as quite active (75−85%) (*14*)].

The visible spectra indicate a fairly minimal disturbance of the hemes when the arginines are mutated, with the exception of the R482P mutation (see below). However, in most of the arginine mutants there is a shift in the EPR band of oxidized heme *a* from $g = 2.83$ to 2.85. Although small, this may be a revealing change, due to the shift ($g = 3.05$) in this direction that is seen in the native bovine oxidase and all other oxidases of the aa_3 type except *Rs* C*c*O and *Pd* C*c*O. Previous studies have concluded that the lower *g* value for *Rs* C*c*O can only be accounted for by proposing a more negative character of one or both of the histidine ligands of heme *a* (*24*). Inspection of the crystal structures of heme *a* in *R. sphaeroides* and bovine C*c*O reveals a difference in the hydrogen bonding of one of the histidine ligands (H102, *R. sphaeroides*; H61, bovine) where a serine (S44, *R. sphaeroides*) (*9*, *10*) replaces a glycine (G30, bovine). This extra hydrogen bond in wild-type *Rs* C*c*O could account for the altered magnetic environment of oxidized heme *a* and for the altered redox potential, which is 40−50 mV less positive in *Rs* C*c*O than bovine (*36*). It is unclear how the mutation of R481 or R482 would alter the magnetic environment of heme *a*, but small perturbations in helix II, which contains H102, or helix I containing S44 could be involved. Decreasing the interaction of S44 with H102 would explain the EPR spectral shift but would suggest a corresponding increase in heme *a* redox potential, whereas a decrease is suggested by the change in *K* (equilibrium constant) (*24*).

It was proposed that R481 is more essential to maintenance of activity in the bo_3 oxidase than R482 (*14*). R481K, although a conservative replacement, would be expected to have a noticeable effect on the structure, as it interacts with the heme a_3 propionates and D412, a ligand of the Mg site, via the peptide backbone. Calculations of an electron transfer pathway from Cu_A to heme *a* predict that R481 does not have a significant role in electron conduction (*19*). R481K C*c*O retains its Mg site, although it is slightly disturbed, and has apparently normal activity when assayed in its isolated form. It also shows normal proton pumping efficiency. It is therefore unlikely that either of the arginines, R481 or R482, are the protonatable sites above the heme *required* for proton exit, although they may still be indirectly involved in proton movement through their organization of water and interaction with the heme propionates (*40*).

Proton pumping has been demonstrated in mutants with low activities [M263L, H260N (*36*), and W143F (*41*)], and so the inhibition of electron transfer alone in R482P is insufficient to explain the lack of proton pumping. The lack of proton pumping in R482P may reflect the disruption of the structure above the hemes that is important in proton release and preventing proton back-leak (*40*).

Rapid Kinetic Studies Explain Decreased Mutant Activity. The R482 mutants, with the exception of R482K, show a decrease in electron transfer rates from cytochrome *c* to Cu_A, k_a, that is parallel to the decreased steady-state activity; i.e., wild type = R482K > R482Q > R482A > R482P (Tables 1 and 3). The rapid electron transfer measurements indicate that R482P has altered the orientation of Ru-55-C*c* at the high-affinity binding site at low ionic strength, such that the rate of electron transfer from cytochrome *c* to Cu_A is decreased ~4000-fold. At higher ionic strength the reorientation of the Ru-55-C*c* allows for more rapid electron transfer,

but the rate of electron transfer (1100 s^{-1}) is maximally still 7-fold less than the wild type (Figure 5). However, because optimum electron transfer occurs at a similar ionic strength for R482P as for the wild type, the binding affinity of Ru-55-C*c* with the R482P mutant is unlikely to be significantly different from the wild type, but rather, the major effect of the R482P mutant appears to be on the orientation of the complex. This is also true to a lesser degree in the other arginine mutants where altered activity is observed. Computational docking of the horse heart cytochrome *c* to bovine C*c*O (*42*) and mutational analysis (*43*, *44*) show that the interaction of C*c* with C*c*O in the C*c*/C*cO* complex involves both subunits I and II of C*c*O. The stability of the subunit I/II interface is likely to be influenced by the presence of Mg, which contains ligands from both subunits ($H411^{I}$, D412 ^{I}, $E254^{II}$, $D229^{II}$). Loss of this metal site in the R482Q, R482A, and R482P may well explain the variable decrease in C*c* to Cu_A electron transfer and decreased Cu_A to heme *a* electron transfer rates. As in R482P, the ionic strength dependence of the cytochrome *c* to Cu_A reaction is only slightly decreased in the R482A mutant, but a perturbed cytochrome *c* binding site is likely due to structural changes at the I/II interface. The Cu_A to heme *a* electron transfer rate in the R482A mutant is faster than that of R482Q, although the cytochrome *c* to Cu_A electron transfer rate is about the same for the two mutants, indicating that these two electron transfer paths are differentially affected by the R482 mutants.

Arginine as Part of an Electron Transfer Pathway? The mutant R482P, like H260N, has a dramatically decreased electron transfer rate from Cu_A to heme *a*, 50 s^{-1} compared to 93000 s^{-1} for the wild type. This large difference in rate cannot be explained by the redox potential difference change. The theoretical value of the rate of electron transfer between Cu_A and heme *a* (k_b), based on the measured redox difference between Cu_A and heme *a* in R482P, is lowered by less than 50%, to 5.5×10^4 s^{-1}, assuming that there is no change in the electronic coupling. Therefore, the low k_b in R482P of 50 s^{-1} is more suggestive of an actual disturbance of the electron transfer pathway from Cu_A to heme *a* or a change in the reorganizational energy involved. It further suggests that, when a single electron is added to oxidized C*c*O, the rate of electron transfer to heme a_3 directly from Cu_A must be much slower than 50 s^{-1}, since no reduction of heme a_3 is observed. One reason for the normally preferential transfer of electrons from Cu_A to heme *a*, rather than heme a_3, is proposed to be a facilitated route of electron transfer in the former case (*45*). A direct electron path from Cu_A to heme *a* (*20*) involving the arginine pair (481/482) and their peptide backbone [14 covalent bonds and 2 hydrogen bonds (*45*)], as well as a low reorganization energy (*18*), has been proposed to result in fast electron transfer rates. Increased reorganizational energy or disruption of this path may slow electron transfer from Cu_A to heme *a*, but it must still be faster than the rate of Cu_A to heme a_3 electron transfer. However, there is good evidence that the redox potential of heme a_3 under these conditions is low (<200 mV) and could prevent significant reduction of heme a_3 regardless of electron transfer rate limitations (*46*).

In R482P, the hydrogen-bonding and charge interactions with the propionate group of heme *a* are undoubtedly broken. Moreover, a shift in the position of the helix XI−XII loop is likely, due to the ring structure of proline; thus, the hydrogen bond of the backbone of Arg481/482 with His260 is likely to be broken. These structural effects could account for the major alterations of the heme sites and the I/II interface in R482P and the significantly decreased electron transfer activities. Indeed, the mutant R482P shows many of the same spectral, structural, and functional alterations as H260N (*36*). This mutation of the Cu_A ligand has a significantly altered redox potential of Cu_A and heme *a*, as well as similarly drastically reduced rates of electron transfer between them (45 s^{-1}), even though the two copper ions are retained in the Cu_A site.

SUMMARY

An intact arginine pair above the hemes is not essential for the proton pumping mechanism, as all of the mutants are capable of proton pumping with the exception of R482P, which is more severely disturbed structurally. However, it appears that there is a need for an arginine at position 482 to maintain the native redox potential of both heme *a* and Cu_A and allow rapid electron transfer between the two metal sites. The data suggest that the interaction between subunits I and II is important for facilitating optimal cytochrome *c*/C*c*O binding and that a part of the role of the Mg site is a longer range influence on structure for cytochrome *c* interaction. The backbone of the helix XI−XII loop in subunit I, which contains R481/482 and interacts closely with subunit II, is likely involved in stabilizing the subunit/subunit interface. More importantly, the arginines and their peptide backbone are part of a protein network whose structure influences the rate of electron transfer across the subunit interface to heme *a*. The data reported here show that the arginine mutations markedly affect the redox potential of heme *a*, most strongly in the case of R482P but also, surprisingly, in the conservative R482K and R481K mutations.

ACKNOWLEDGMENT

We thank Rashida Morgan and Amanda Looney for help with making the site-directed mutants.

REFERENCES

1. Michel, H. (1998) The mechanism of proton pumping by cytochrome *c* oxidase, *Proc. Natl. Acad. Sci. U.S.A. 95*, 12819−12824.
2. Hofacker, I., and Schulten, K. (1998) Oxygen and proton pathways in cytochrome *c* oxidase, *Proteins 30*, 100−107.
3. Verkhovskaya, M. L., Garcia-Horsman, A., Puustinen, A., Rigaud, J. L., Morgan, J. E., Verkhovsky, M. I., and Wikstrom, M. (1997) Glutamic acid 286 in subunit I of cytochrome bo_3 is involved in proton translocation, *Proc. Natl. Acad. Sci. U.S.A. 94*, 10128−10131.
4. Lubben, M., Prutsch, A., Mamat, B., and Gerwert, K. (1999) Electron transfer induces side-chain changes of glutamate-286 from cytochrome bo_3, *Biochemistry 38*, 2048−2056.
5. Rost, B., Behr, J., Hellwig, P., Richter, O.-M. H., Ludwig, B., Michel, H., and Mantele, W. (1999) Time-resolved FT-IR studies on the CO adduct of *Paracoccus denitrificans* cytochrome *c* oxidase: comparison of the fully reduced and the mixed valence form, *Biochemistry 38*, 7565−7571.
6. Rich, P., Meunier, B., Mitchell, R., and Moody, R. (1996) Coupling of charge and proton movement in cytochrome *c* oxidase, *Biochim. Biophys. Acta 1275*, 91−95.
7. Louro, R. O., Catarino, T., LeGall, J., Turner, D. L., and Xavier, A. V. (2001) Cooperativity between electrons and proton in monomeric cytochrome c_3: The importance of mechano-chemical coupling for energy transduction, *ChemBioChem 2*, 831−837.

8. Iwata, S., Ostermeier, C., Ludwig, B., and Michel, H. (1995) Structure at 2.8 Å resolution of cytochrome *c* oxidase from *Paracoccus denitrificans*, *Nature 376*, 660−669.
9. Tsukihara, T., Aoyama, H., Yamashita, E., Tomizaki, T., Yamaguchi, H., Shinzawa-Itoh, K., Nakashima, R., Yaono, R., and Yoshikawa, S. (1996) The whole structure of the 13-subunit oxidized cytochrome *c* oxidase at 2.8 Å, *Science 272*, 1136−1144.
10. Svensson-Ek, M., Abramson, J., Larsson, G., Tornoth, S., Brzezinski, P., and Iwata, S. (2002) The X-ray crystal structures of wild-type and EQ(I-286) mutant cytochrome *c* oxidases from *Rhodobacter sphaeroides*, *J. Mol. Biol. 321*, 329−339.
11. Florens, L., Schmidt, B., McCracken, J., and Ferguson-Miller, S. (2001) Fast deuterium access to the buried magnesium/manganese site in cytochrome *c* oxidase, *Biochemistry 40*, 7491−7497.
12. Florens, L., Hoganson, C., McCracken, J., Fetter, J., Mills, D. A., Babcock, G. T., and Ferguson-Miller, S. (1999) in *The Phototropic Prokaryotes* (Peschek, G., Löffelhard, W., and Schmetterer, G., Eds.) pp 329−339, Kluwer Academic/Plenum Publishers, New York.
13. Mills, D. A., Florens, L., Hiser, C., Qian, J., and Ferguson-Miller, S. (2000) Where is "outside" in cytochrome *c* oxidase and how and when do protons get there?, *Biochim. Biophys. Acta 1458*, 180−187.
14. Puustinen, A., and Wikstrom, M. (1999) Proton exit from the heme-copper oxidase of *Escherichia coli*, *Proc. Natl. Acad. Sci. U.S.A. 96*, 35−37.
15. Pan, L. P., Hibdon, S., Liu, R.-Q., Durham, B., and Millett, F. (1993) Intracomplex electron transfer between ruthenium-cytochrome *c* derivatives and cytochrome *c* oxidase, *Biochemistry 32*, 8492−8498.
16. Geren, L. M., Beasley, J. R., Fine, B. R., Saunders, A. J., Hibdon, S., Pielak, G. J., Durham, B., and Millett, F. (1995) Design of a ruthenium-cytochrome *c* derivative to measure electron transfer to the initial acceptor in cytochrome *c* oxidase, *J. Biol. Chem. 270*, 2466−2662.
17. Winkler, J. R., Malmstrom, B. G., and Gray, H. B. (1995) Rapid electron injection into multisite metalloproteins: intramolecular electron transfer in cytochrome oxidase, *Biophys. Chem. 54*, 199−209.
18. Brzezinski, P. (1996) Internal electron transfer reactions in cytochrome *c* oxidase, *Biochemistry 35*, 5612−5615.
19. Zheng, X., Medvedev, D. M., Swanson, J., and Stuchebrukhov, A. A. (2003) Computer simulation of water in cytochrome *c* oxidase, *Biochim. Biophys. Acta 1557*, 99−107.
20. Ramirez, B. E., Malmstrom, B. G., Winkler, J. R., and Gray, H. B. (1995) The currents of life: The terminal electron transfer complex of respiration, *Proc. Natl. Acad. Sci. U.S.A. 92*, 11949−11951.
21. Moser, C. C., Page, C. C., Farid, R., and Dutton, P. L. (1995) Biological electron transfer, *J. Bioenerg. Biomembr. 27*, 263−274.
22. Horton, R. M., Hunt, H. D., Ho, S. N., Pullen, J. K., and Pease, L. R. (1989) Enginering hybrid genes without the use of restriction enzymes: gene splicing by overlap extension, *Gene 77*, 61−68.
23. Mitchell, D. M., and Gennis, R. B. (1995) Rapid purification of wildtype and mutant cytochrome *c* oxidase from *Rhodobacter sphaeroides* by Ni^{2+}-NTA affinity chromatography, *FEBS Lett. 368*, 148−150.
24. Qian, J., Shi, W., Pressler, M., Hoganson, C., Mills, D., Babcock, G. T., and Ferguson-Miller, S. (1997) Aspartate-407 in *Rhodobacter sphaeroides* cytochrome *c* oxidase is not required for proton pumping or Mn binding, *Biochemistry 36*, 2539−2543.
25. Hosler, J. P., Fetter, J., Tecklenburg, M. M. J., Espe, M., Lerma, C., and Ferguson-Miller, S. (1992) Cytochrome aa_3 of *Rhodobacter sphaeroides* as a model for mitochondrial cytochrome *c* oxidase, *J. Biol. Chem. 267*, 24264−24272.
26. Fetter, J. R., Qian, J., Shapleigh, J., Thomas, J. W., García-Horsman, J. A., Schmidt, E., Hosler, J., Babcock, G. T., Gennis, R. B., and Ferguson-Miller, S. (1995) Possible proton relay pathways in cytochrome *c* oxidase, *Proc. Nat. Acad. Sci. U.S.A. 92*, 1604−1608.
27. Zhen, Y., Qian, J., Follmann, K., Hosler, J., Hayward, T., Nilsson, T., and Ferguson-Miller, S. (1998) Overexpression and purification of cytochrome *c* oxidase from *Rhodobacter sphaeroides*, *Protein Expression Purif. 13*, 326−336.
28. Hiser, C., Mills, D. A., Schall, M., and Ferguson-Miller, S. (2001) C-terminal truncation and histidine-tagging of cytochrome *c* oxidase subunit II reveals the native processing site, shows involvement of the C-terminus in cytochrome *c* binding, and improves the assay for proton pumping, *Biochemistry 40*, 1606−1615.
29. Brunori, M., Sarti, P., Colosimo, A., Antonini, G., Malatesta, F., Jones, M., and Wilson, M. (1985) Mechanism of control of cytochrome *c* oxidase activity by the electrochemical-proton gradient, *EMBO J. 4*, 2365−2368.
30. Wang, K., Mei, H., Geren, L., Miller, M. A., Saunders, A., Wang, X., Waldner, J. L., Pielak, G. J., Durham, B., and Millett, F. (1996) Design of a ruthenium-cytochrome *c* derivative to measure electron transfer to the radical cation and oxyferryl heme in cytochrome *c* peroxidase, *Biochemistry 35*, 15107−15119.
31. Margoliash, E., and Frohwirt, N. (1959) Spectrum of horse-heart cytochrome *c*, *Biochem. J. 71*, 570.
32. Blair, D. F., Martin, C. T., Gelles, J., Wang, H., Brudvig, G. W., Stevens, T. H., and Chan, S. I. (1983) The metal centers of cytochrome *c* oxidase: structures and interactions, *Chem. Scr. 21*, 43−53.
33. Blair, D. F., Bocian, D. F., Babcock, G. T., and Chan, S. I. (1982) Evidence for modulation of the heme absorptions of cytochrome *c* oxidase by metal−metal interactions, *Biochemistry 21*, 6928−6935.
34. Greenwood, C., Hill, B. C., Barber, D., Eglinton, D. G., and Thomson, A. J. (1983) The optical properties of Cu_A in bovine cytochrome *c* oxidase determined by low-temperature magnetic-circular-dichroism spectroscopy, *Biochem. J. 215*, 303−316.
35. Espe, M. P., Hosler, J. P., Ferguson-Miller, S., Babcock, G. T., and McCracken, J. (1995) A continuous wave and pulsed EPR characterization of the Mn^{2+} binding site in *Rhodobacter sphaeroides* cytochrome *c* oxidase, *Biochemistry 34*, 7593−7602.
36. Zhen, Y., Schmidt, B., Kang, U. G., Antholine, W., and Ferguson-Miller, S. (2002) Mutants of the Cu_A site in cytochrome *c* oxidase of *Rhodobacter sphaeroides*: I. Spectral and functional properties, *Biochemistry 41*, 2288−2297.
37. Wang, K., Zhen, Y., Sadoski, R., Grinnell, S., Geren, L., Ferguson-Miller, S., Durham, B., and Millett, F. (1999) Definition of interaction domain for the reaction of cytochrome *c* with cytochrome *c* oxidase: II. Rapid kinetics analysis of electron transfer from cytochrome *c* to *Rhodobacter sphaeroides* cytochrome oxidase surface mutants, *J. Biol. Chem. 274*, 38042−38050.
38. Durham, B., Pan, L. P., Long, J. E., and Millett, F. (1989) Photoinduced electron transfer kinetics of singly labeled ruthenium bis(bipyridine) dicarboxybipyridine cytochrome *c* derivatives, *Biochemistry 28*, 8659−8665.
39. Zaslavsky, D., Sadoski, R. C., Wang, K., Durham, B., Gennis, R. B., and Millett, F. (1998) Single electron reduction of cytochrome *c* oxidase compound F: resolution of partial steps by transient spectroscopy, *Biochemistry 37*, 14910−14916.
40. Mills, D. A., Schmidt, B., Hiser, C., Westley, E., and Ferguson-Miller, S. (2002) Membrane potential-controlled inhibition of cytochrome *c* oxidase by zinc, *J. Biol. Chem. 277*, 14894−14901.
41. Mills, D. A., Tan, Z., Ferguson-Miller, S., and Hosler, J. (2003) A role for subunit III in proton uptake into the D pathway and a possible proton exit pathway in *Rhodobacter sphaeroides* cytochrome *c* oxidase, *Biochemistry 42*, 7410−7417.
42. Roberts, V. A., and Pique, M. E. (1999) Definition of the interaction domain for cytochrome *c* on cytochrome *c* oxidase: III. Calculation of the docked complex, *J. Biol. Chem. 274*, 38051−38060.
43. Zhen, Y., Hoganson, C. W., Babcock, G. T., and Ferguson-Miller, S. (1999) Definition of interaction domain for the reaction of cytochrome *c* with cytochrome *c* oxidase: I. Biochemical, spectral and kinetic characterization of surface mutants in subinit II of *Rhodobacter sphaeroides* cytochrome aa_3, *J. Biol. Chem. 274*, 38032−38041.
44. Witt, H., Zickermann, V., and Ludwig, B. (1995) Site-directed mutagenesis of cytochrome *c* oxidase reveals two acidic residues involved in the binding of cytochrome *c*, *Biochim. Biophys. Acta 1230*, 74−76.
45. Regan, J. J., Ramirez, B. E., Winkler, J. R., Gray, H. B., and Malmstrom, B. G. (1998) Pathways for electron tunneling in cytochrome *c* oxidase, *J. Bioenerg. Biomembr. 30*, 35.
46. Verkhovsky, M. I., Morgan, J. E., and Wikstrom, M. (1995) Control of electron delivery to the oxygen reduction site of cytochrome *c* oxidase: A role for protons, *Biochemistry 34*, 7483−7491.

BI036279O